Journal of CO_2 Utilization 34 (2019) 646–655

Contents lists available at ScienceDirect

Journal of CO_2 Utilization

journal homepage: www.elsevier.com/locate/jcou

CO_2 sequestration coupled with enhanced gas recovery in shale gas reservoirs

Erfan Mohagheghian, Hassan Hassanzadeh*, Zhangxin Chen

Department of Chemical & Petroleum Engineering, Schulich School of Engineering, University of Calgary, Calgary, AB, T2N 1N4, Canada

ARTICLE INFO

Keywords:
Shale gas reservoir
CO_2 sequestration
CO_2-EGR
Enhanced gas recovery
Sorption
Adsorbed phase trapping

ABSTRACT

Carbon capture and storage in depleted shale gas reservoirs offers an opportunity to utilize CO_2 for enhanced gas recovery while providing access to fossil fuels. To evaluate CO_2 sequestration coupled with enhanced gas recovery (CO_2-EGR), we have developed a model that takes into account all the major contributing mechanisms in shale gas dynamics including viscous flow, gas slippage, Knudsen diffusion, competitive adsorption of different components, pore size variation and real gas effect. The CO_2-EGR process is divided into periods of primary production, CO_2 injection, soaking and secondary simultaneous production of CO_2 along with other natural gas components. Numerical simulations are conducted to study the feasibility of CO_2 sequestration and enhanced gas recovery and analyze the response of the shale gas reservoir to input variables including reservoir pressure, temperature and intrinsic permeability. The results show that the stronger adsorption of CO_2 over CH_4 molecules to shale surface is the main influencing mechanism on CO_2 sequestration. It is shown that 30–55% percent of the injected CO_2 can be trapped as adsorbed phase in shale while providing 8–16% incremental gas recovery. Comparing trapping efficiency of CO_2-EGR with other methods of accelerating CO_2 dissolution in deep saline aquifers, adsorbed phase trapping is promising.

1. Introduction

Global warming caused by the emission of anthropogenic carbon dioxide (CO_2) and other greenhouse gases has become a major challenge faced by industrial countries. CO_2 capture and storage (CCS) in geological formations as an option to mitigate emission has attracted a great deal of attention [1–3]. Depleted oil and gas reservoirs [4–7], deep saline aquifers [8], unmineable coalbeds [9], gas hydrates [10] and depleted shale gas reservoirs [11] are the main geological targets for CO_2 storage. Capture and geological storage has the potential to reduce the global carbon dioxide emissions significantly if the technologies are utilized efficiently [12].

Among the noted options, storage in oil and gas shales has been relatively less studied. While the infrastructures for extraction of shale gas exist or are currently under development, integration of geological storage of CO_2 with gas recovery from these formations provides unique opportunities for reduction of CO_2 emissions.

Unconventional reservoirs such as gas shales are distributed over the world and are considered as an abundant alternative source of energy with a technically recoverable amount of approximately 7800trillion cubic feet (TCF) of gas [13]. The recent advances in horizontal drilling and hydraulic fracturing technology have made production from shale reservoirs an economically viable option [14,15]. The gas, mainly methane, is stored in shale in the form of free gas, adsorbed gas or dissolved in the kerogen [16]. The free gas exists in the pore space and natural fractures. The adsorbed gas is attached to the internal surface of shale if the attractive forces between the gas molecules and solid surface are greater than those between the molecules [17]. The adsorption capacity depends on the total organic carbon (TOC) content of shale and the clay minerals and the adsorbed phase could contribute to the total gas in place in the range of 20 to 85% [18]. The dissolved gas in kerogen is released and diffused into the porous structure of shale upon pressure decline [19].

CO_2 can be permanently stored in depleted shale gas reservoirs as shale plays could act as impermeable barriers and prevent CO_2 leakage. The storage mechanisms of CO_2 in shale include hydrodynamic, adsorption, solution, and residual or capillary trapping. Adsorption trapping is quite critical for CO_2 storage and the adsorbed gas is unlikely to escape over geological time spans. The abundance of shale formations over the world as well as the high adsorption affinity of CO_2 for shale indicate the larger storage potential of shale reservoirs compared to the alternatives [20].

CO_2 sequestration in gas shale formations can be coupled with enhanced methane recovery so as to compensate for the cost of storage.

* Corresponding author.
E-mail address: hhassanz@ucalgary.ca (H. Hassanzadeh).

https://doi.org/10.1016/j.jcou.2019.08.016
Received 17 July 2019; Received in revised form 10 August 2019; Accepted 20 August 2019
Available online 31 August 2019

The economic potential estimate of CO_2 sequestration enhanced gas recovery (CO_2-EGR) is about 280 *Gt* CO_2 storage and 2500 *TCF* additional methane recovery [21]. Kang et al. [22] measured the adsorption capacity of CO_2 and CH_4 on two Barnett shale samples and the amount of CO_2 adsorption was reported to be five to ten times greater than that of CH_4; noting that the adsorption isotherm for both of the components followed Langmuir adsorption model.

Many researchers have investigated CO_2 sequestration in shale gas reservoirs. An economic feasibility evaluation of CO_2 storage in depleted shale gas formations was conducted by Tayari et al. [23]. CO_2 storage capacity varies over the range of 5 to 10 kg per tonne of shale, hence shale gas reservoirs were suggested as potential candidates of CO_2 sequestration by Boosari et al. [24] Chareonsuppanimit et al. [25] measured the adsorption capacity of CO_2, CH_4 and N_2 on New Albany shale samples at $328K$ and pressures up to $1800psia$ by means of a volumetric set-up and analyzed the results using a simplified local density adsorption model. The adsorption capacity of CO_2 was by far the highest, followed by CH_4 and N_2. Kang et al. [22] carried out scanning electron microscope (SEM) experiments and numerical studies on Forth Worth basin shale samples and claimed that up to 97% of the stored CO_2 in shale is in the adsorbed phase inside the organic pores depending on the reservoir pressure. Fathi and Akkutlu [26] numerically simulated CO_2 injection into shale gas reservoirs and proposed it as an enhanced gas recovery method due to the preferential adsorption of CO_2 over CH_4. Sun et al. [27] developed a dual porosity mathematical model for CO_2-EGR in shale gas reservoirs using COMSOL software and included the effects of viscous flow, Knudsen and ordinary diffusion as well as gas desorption from the matrix. However, the slip coefficient (Klinkenberg factor) is not pressure dependent in their analysis.

The pore diameter in shale gas reservoirs is in the range of 1 to $200nm$,the permeability is extremely low [28–30] and several transport mechanisms contribute to the flow and therefore the complexity of the system invalidates the assumptions of Navier-Stokes equations and Darcy's law [31,32]. The main involved mechanisms in shale gas flow dynamics include viscous flow of the free gas, gas desorption from matrix surface which is a major contributor after pressure drops below the critical sorption pressure [33–36], slip flow [32], Knudsen diffusion due to the comparability of the pore size and the mean free path of gas molecules [28], and pore enlargement as the result of shale pore compressibility [37]. It is established that gas production rates in shale media are higher than the values predicted by Darcy's law caused by the combined effects of the above mechanisms [29].

A comprehensive modelling which is capable of simulating the effects of all the involved mechanisms is a complicated and computationally demanding task and is beyond the capability of the existing commercial numerical reservoir simulators. In this paper, we present our model incorporating the effects of the above contributing mechanisms, namely viscous flow, slip flow (Klinkenberg effect), Knudsen diffusion, adsorption/desorption, pore radius change and real gas effect on multi-component shale gas transport. The reservoir model is set for CO_2-EGR simulation including periods of primary depletion, CO_2 injection, soaking and secondary production, and several case studies are solved numerically. The performance of CO_2 sequestration coupled with enhanced gas recovery, the effects of pressure and temperature on the operation especially in the presence and absence of sorption for different permeabilities and variation of gas concentration in the medium are investigated. The proposed model is novel in the sense that it captures the overall effect of all the involved mechanisms in shale gas flow while measuring the sensitivity of CO_2-EGR to various in-situ parameters. The contribution of adsorption to methane replacement by carbon dioxide is measured separately from the free gas portion and sensitivity analysis on changing permeability, pressure and temperature including and excluding adsorption is conducted. The concentrations of various gas components which reveal the proportion of trapped CO_2 in adsorbed phase and additional methane recovered are presented as normalized dimensionless values. The simultaneous effects of all the mentioned transport mechanisms and the exhaustive set of experiments have not been examined before to the best of our knowledge.

2. Mathematical formulation

2.1. Transport model of multi-component gas in shale media

The mechanisms involved in multi-component shale gas transport include viscous flow, slip flow, Knudsen and ordinary diffusion. The dusty-gas model (DGM) is capable to cope with the diffusion mechanisms using kinetic theory of gases [38], however the interactions between the molecules make the system of partial differential equations demanding and difficult to solve.

Viscous flow is caused by the collisions between the molecules, while Knudsen diffusion is generated by the collisions of the molecules with the pore walls. When the pore size is in the same order of magnitude as the mean free path of the molecules, Knudsen diffusion is more pronounced. At nano scale of shale porous media, both viscous flow and Knudsen diffusion influence gas transport.

The model used in this study is adapted from our previous paper [39] and is the extended version of the equations developed in [40]. The flux of gaseous component i in shale pore space denoted as$\vec{F_i}$ is presented as follows.

$$\vec{F_i} = -y_i\rho\frac{k_D}{\mu}\left(1+\frac{b_i}{P}\right)\vec{\nabla}P - \frac{D_{kn,i}}{RT}\vec{\nabla}\left(\frac{Py_i}{Z}\right), \tag{1}$$

where y_i is the mole fraction of component i,ρ is the molar density of the gas mixture, k_D is Darcy (intrinsic) permeability, μ is gas viscosity, b_i is the Klinkenberg parameter for component i, which incorporates slip flow into the model, $D_{kn,i}$ is the effective Knudsen diffusivity of component iP is pressure, R is the universal gas constant, T is temperature and Z is gas compressibility or deviation factor.

Peng-Robinson equation of state [40] and Lee correlation [41] are used to update the compressibility factor and gas viscosity, respectively, versus pressure and composition.

The Klinkenberg parameter of component i is formulated as below.

$$b_i = \sqrt{\frac{8\pi RT}{M_i}}\frac{\mu}{r_{eff}}\left(\frac{2}{\alpha_i}-1\right), \tag{2}$$

where M_i is the molar mass of component i and r_{eff} refers to the effective pore radius, which dynamically varies versus changes of pressure and composition in the course of simulations.

The effective pore radius is adjusted with pressure and composition using Langmuir adsorption as shown in the following equation [37].

$$r_{eff} = \sqrt{\frac{8\tau k_D}{\phi}} - \sum_{i=1}^{Nc}\frac{\delta_i\frac{Py_i}{P_{L,i}}}{1+P\sum_{j=1}^{Nc}\frac{y_j}{P_{L,j}}}, \tag{3}$$

The first term on the right side represents the average pore radius [42], $\delta_i$is the diameter of molecule i,ϕ and τ are the porosity and tortuosity of shale medium [43], respectively.

Parameterα_i is the tangential momentum accommodation coefficient (TMAC) of component i which has been correlated by Agrawal and Prabhu [44] and extended to capture the coexistence of multiple components.

$$\alpha_i = 1 - \log(1+Kn_i^{0.7}), \tag{4}$$

where Kn_i is the Knudsen number of component i,which is included to account for the comparability of the pore size and the mean free path of the gas molecules. This factor depends on the effective pore radius, pressure, temperature and the molecule diameter.

$$Kn_i = \frac{k_B T}{\pi\sqrt{2}\,r_{eff}\,\delta_i^2 P}, \tag{5}$$

where $k_B$is Boltzmann constant.

The effective Knudsen diffusivity of component i ($D_{kn,i}$),presented in the following equation is the modified molecular diffusion including the effects of porosity and tortuosity [45].

$$D_{kn,i} = \frac{16}{3}\sqrt{\frac{RTk_D\phi}{\pi M_i \tau}}. \tag{6}$$

2.2. Gas adsorption/desorption equation

As pressure drops to critical sorption pressure due to free gas production, the adsorbed gas is liberated from shale surface and produced [37]. The extended Langmuir isotherm adsorption model is well capable to model and predict adsorption of different gaseous components on shale [36]. The moles of adsorbed component i on shale unit volume ($q_{a,i}$) is presented as follows in Langmuir model.

$$q_{a,i} = \frac{\rho_s P^{sc}}{RT^{sc}} \frac{V_{L,i}\frac{Py_i}{P_{L,i}}}{1 + P\sum_{j=1}^{Nc}\frac{y_j}{P_{L,j}}}, \tag{7}$$

where ρ_s is the shale density, P^{sc} and $T^{sc}$are standard pressure and temperature, respectively, $V_{L,i}$and $P_{L,i}$ are the Langmuir volume and Langmuir pressure of component i,respectively, and $N_c$is the number of components.

2.3. Continuity equation of matrix

The gaseous components exist in shale matrix both as free and adsorbed phase, so the mechanisms of free gas transport in addition to desorption must be taken into account in the matrix. According to mass conservation law, the continuity of component i in the matrix assuming constant porosity can be written as follows.

$$\phi\frac{\partial}{\partial t}(\rho y_i) + (1-\phi)\frac{\partial}{\partial t}q_{a,i} = -\vec{\nabla}.\vec{F_i}. \tag{8}$$

Using Eq. (1) to obtain the flow vector term in a 1D linear model including mechanisms of viscous flow, slip flow and Knudsen diffusion, by applying extended Langmuir equation for adsorbed gas and real gas law for molar density ($\rho = P/ZRT$) and assuming isothermal flow, the final form of continuity equation for multi-component single-phase gas in shale matrix is derived as below.

$$\phi\frac{\partial}{\partial t}\left(\frac{Py_i}{Z}\right) + \frac{(1-\phi)\rho_s TP^{sc}V_{L,i}}{T^{sc}P_{L,i}}\frac{\partial}{\partial t}\left(\frac{Py_i}{1 + P\sum_{j=1}^{Nc}\frac{y_j}{P_{L,j}}}\right) = \frac{\partial}{\partial x}\left[\frac{y_i}{Z}\frac{k_D}{\mu}(P+b_i)\frac{\partial P}{\partial x} + D_{kn,i}\frac{\partial}{\partial x}\left(\frac{Py_i}{Z}\right)\right]. \tag{9}$$

2.4. Model inputs, initial and boundary conditions

The initial pressure P_i and temperature T_i of the model as well as Darcy permeability k_D are selected for sensitivity measurements. Table 1 presents some of the model inputs. The initial composition of gas in place is also shown in the Table 1. Langmuir volumes are 9.8×10^{-4} and $1.91 \times 10^{-3} m^3/kg$, and Langmuir pressures are 3.05 and 1.68MPa for CH_4 and CO_2, respectively, for the base case that will be defined later. We assume one dimensional model where the left boundary is under no-flow condition and constant pressure of 1000$psia$ and zero concentration gradient are set at the right end of the model.

Table 1
Input parameters used in the reservoir model.

Property	Value
Porosity, ϕ[−]	0.1
Length, L [m]	4
Outlet boundary pressure [$psia$]	1000
Tortuosity, τ[−]	4
Initial mole fraction of C_1, C_2, C_3, CO_2	(y_i = 0.6, 0.25, 0.1, 0.05)

3. Verification and methodology

3.1. Verification of the numerical solution and developed model

The mathematical model for each component in shale gas matrix system is presented in Eq. (9). This model is a function of pressure and mole fractions of ($N_c - 1$) components, taking into account that mole fractions add up to unity($\sum_{i=1}^{N_c} y_i = 1$). The number of unknown dependent variables is N_c per each of the N_b grid blocks and a linear system of $N_c \times N_b$dimensions must be solved per time step and advance in time. Implicit Euler in time and centered differences in space are used to discretize the equations, single-point upstream weighting is applied to obtain the estimated values of the parameters at the blocks interface, and the Newton-Raphson iterative method is employed as the nonlinear solver with the maximum iterations of 30 and the tolerance factor of 10^{-4} for the norm of the residual vector.

Since the available commercial numerical reservoir simulators cannot take into account the coupling mechanisms of gas transport in shale media, namely viscous flow, Knudsen diffusion, slip flow and sorption, and there is no analytical solution to the above problem, in order to verify the accuracy of the numerical method, viscous flow of single component gas in porous medium was simulated by nullifying the effects of other physical phenomena in the numerical code and the solution was validated against the analytical solution of gas diffusivity equation (pseudo-potential function). Furthermore, the accuracy and validity of the developed model has also been tested and confirmed in our previous paper on the applicability of the concept of shale apparent permeability [39].

3.2. Methodology

Due to the competitive adsorption of CO_2 over CH_4 to the shale matrix, partially depleted shale gas reservoirs are potential candidates for CO_2 sequestration coupled with enhanced gas recovery (CO_2-EGR). In this study, the developed model described in the previous section is employed to test the feasibility and applicability of CO_2-EGR in shale gas media coupling the transport mechanisms of viscous flow, slip flow, Knudsen diffusion, adsorption/desorption and pore radius change. The simulation scenarios include a period of primary depletion for 120 days followed by CO_2 injection for 30 days, a short soaking period of 10 days followed by secondary production period of 60 days over which CO_2 and CH_4 are produced simultaneously. The dynamics of the above stages are investigated in several case studies in which initial pressure of the medium, temperature and Darcy permeability in the presence and absence of sorption mechanism are varied systematically as sensitivity analysis measures and the results are compared, analyzed and discussed in the following sections.

4. Results and discussion

The three parameters of initial pressure, temperature and Darcy permeability are selected for sensitivity studies and to investigate the performance and potential of CO_2-EGR in shale gas reservoirs. Three levels for initial pressure, three levels for the medium temperature and three levels for permeability are considered and each simulation scenario is conducted both including and excluding the effect of sorption. The values of the above parameters for the base case are 4500$psia$ as the initial reservoir pressure, 75°C as the temperature and Darcy permeability of 100nD, and the initial gas in place is calculated to be around 4900 moles. In each scenario, after 120 days of primary production, CO_2 is injected into the medium with a constant rate of 0.001mol/s, the well

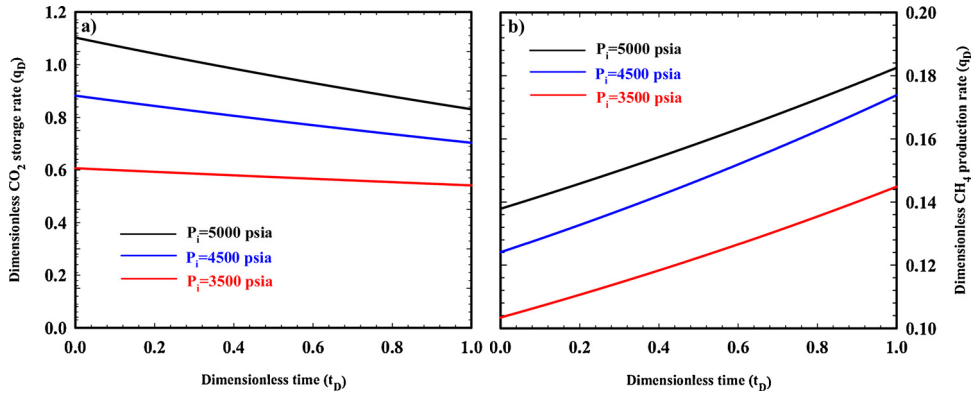

Fig. 1. CO_2 storage and CH_4 production rates versus dimensionless time for three different initial reservoir pressures; the CO_2 storage rate declines and the production rate of methane grows with time. The slope of the curves is greater at higher initial pressures.

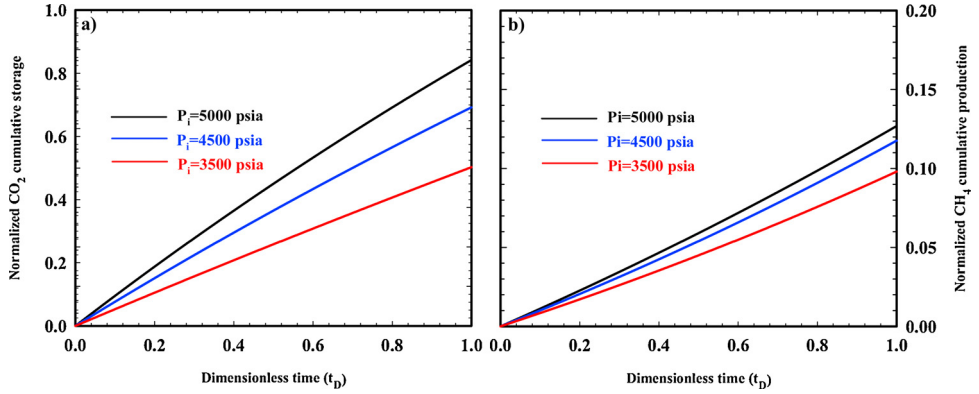

Fig. 2. Normalized cumulative CO_2 storage and CH_4 production versus dimensionless time for three different initial reservoir pressures; the ratio of the former to the latter quantity is ascending versus pressure and varies between five and seven for the range of pressure studied in this work.

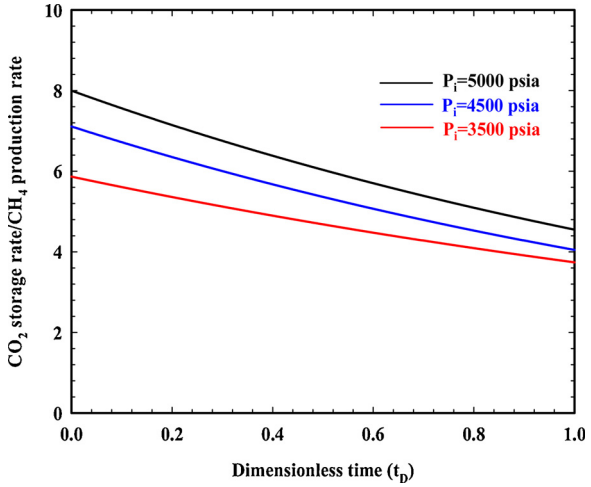

Fig. 3. The ratio of CO_2 storage to CH_4 production rates versus time; this ratio is higher at higher pressures, the initial rate of decline and the late-time ratio are close for different pressures.

is shut down (soaking) for a period of 10 days and then put on secondary production for the next 60 days. The pressures and concentrations at the end of each stage are used as the initial conditions for the next stage. The influence of each of the above parameters as well as sorption on the dynamics of CO_2 sequestration and CH_4 recovery during CO_2-EGR is studied and the results are presented and discussed in what follows.

4.1. Effect of initial pressure on CO_2 sequestration and CH_4 recovery

It is worth restating that the injections are performed at a constant equal rate for the same period of time in all the cases; therefore, same amount of CO_2 is added to the reservoir at the end of the injection period. To better scale the problem, we define dimensionless storage/production rate as $q_D = q_k t_p/G$ and dimensionless time as $t_D = q_{inj} t/G$, where q_k is the rate of methane production/CO_2 storage during secondary production, q_{inj} is CO_2 injection rate and $G$is the initial gas in place, all in consistent system of units.

Fig. 1 illustrates normalized CO_2 storage and CH_4 production rates versus dimensionless time for three different initial pressures. The CO_2 storage here counts both for the gas stored in free phase as well as the adsorbed phase and the CH_4 produced also includes the total of desorbed and free gas. The temperature and Darcy permeability are set at $75°C$ and $100nD$,respectively. Since higher initial pressure translates to higher pressure at the end of primary production, in order for the same amount of CO_2 to be injected into the reservoir, injection pressure must be higher when the initial pressure is higher. Intuitively, more CO_2 is stored when the injection pressure, i.e., initial pressure is higher. As a result, more CH_4 is desorbed and displaced by CO_2 due to stronger adsorption of CO_2 to shale surface compared to methane. At higher initial pressures, the decline of CO_2 storage rate is faster and accordingly methane production rate rises more quickly. As can be noticed in Fig. 2, normalized CO_2 cumulative storage, which is defined as the ratio of the total stored to the total injected CO_2, is far greater than normalized CH_4 cumulative production (the ratio of the total produced to the initial CH_4 in place) in general regardless of the initial pressure. At the initial pressure of $5000psia$,85% of the total injected CO_2 is stored and around 12% of the initial methane in place is produced during the secondary recovery. In other words, CO_2 storage is seven times greater

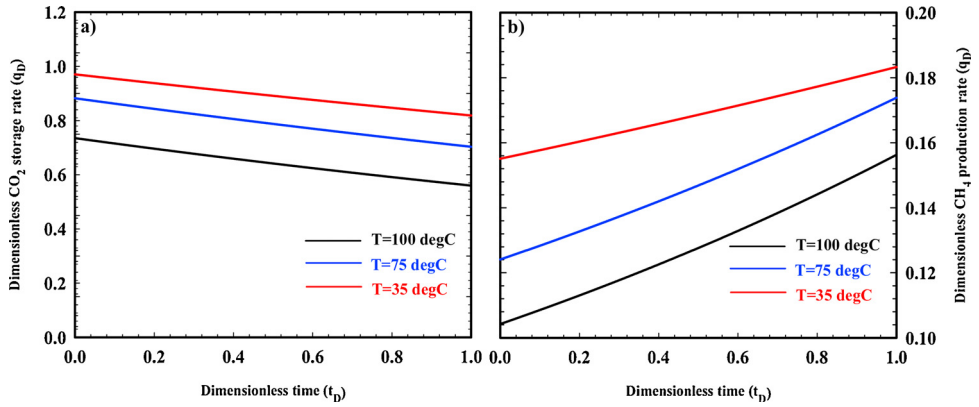

Fig. 4. CO_2 storage and CH_4 production rates at three different reservoir temperatures; increasing the temperature lowers both the storage and production rate. The changes happen more rapidly or the slopes are greater at higher temperatures.

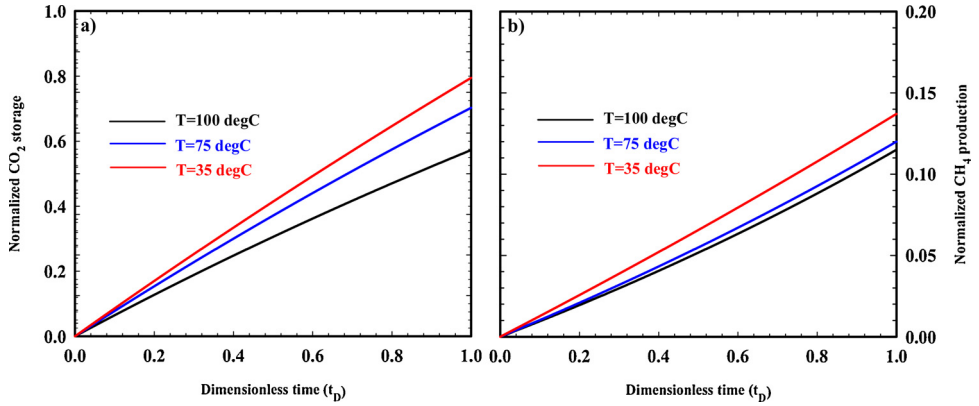

Fig. 5. Normalized cumulative CO_2 storage and CH_4 production versus time for three different reservoir temperatures; reducing temperature from 100°C to 35°C, increases final cumulative methane recovery by 2.3%, however a boost of 24% is achieved in final cumulative CO_2 storage.

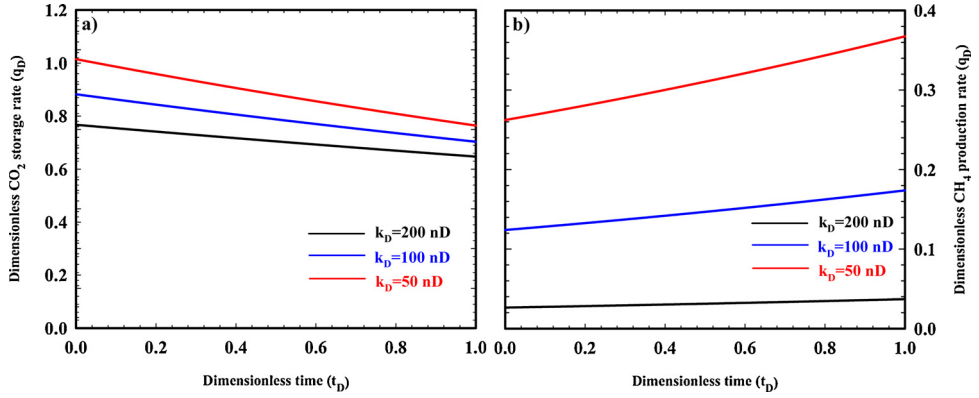

Fig. 6. CO_2 storage and CH_4 production rates at three different reservoir intrinsic permeabilities; decreasing the Darcy permeability leads to growth in both the storage and production rate. The decline of CO_2 storage rate with time is more noticeable at lower permeabilities.

than CH_4 additional recovery. At lower pressures this ratio decreases; however, still far beyond one (5: 1 at the initial pressure of 3500psia). This indicates the high potential of shale gas reservoirs to store large amounts of CO_2 as a greenhouse gas. It is seen that in all cases, more than 50% of the injected CO_2 has been trapped in the reservoir.

The variation of the ratio of CO_2 storage to CH_4 production rate with time is depicted in Fig. 3. As the injection pressure increases, for the same production rate of CH_4, more CO_2 can be stored in the shale gas reservoir. This ratio decreases over time since CO_2 storage rate declines and CH_4 production rate grows versus time as shown in Fig. 1.

4.2. *Effect of reservoir temperature on CO_2 sequestration and CH_4 recovery*

Three distinct temperatures are chosen to investigate the effect of temperature on the performance of CO_2-EGR in shale gas reservoirs. The selected temperatures are above the critical temperature of CO_2 to assure the existence of single-phase gas in the reservoir throughout the simulations. The initial reservoir pressure and intrinsic permeability are set at the values assumed for the base case. As temperature reduces, the maximum amount of gas adsorbed on the shale surface (Langmuir volume) decreases. Therefore, it is expected that at higher temperatures less CO_2 is adsorbed and consequently less CH_4 is replaced by CO_2 molecules; in other words, CO_2 storage and CH_4 additional recovery

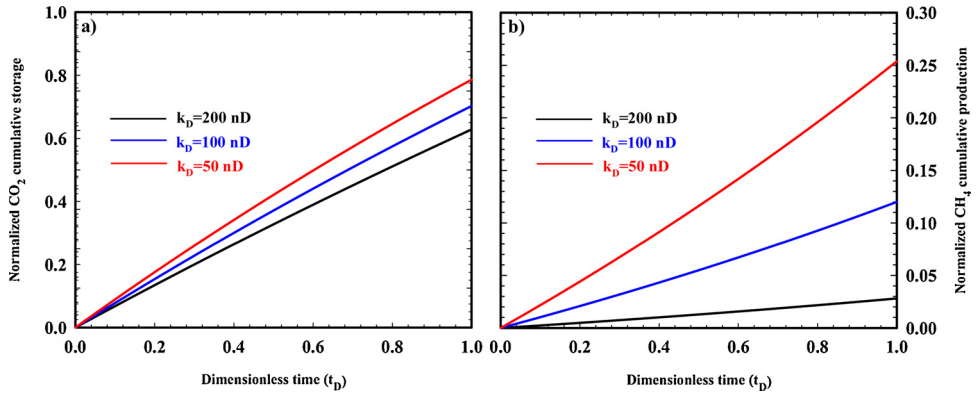

Fig. 7. Normalized cumulative CO_2 storage and CH_4 production versus time for three different reservoir Darcy permeabilities; reducing intrinsic permeability from 200*nD* to 50*nD*, increases final cumulative methane recovery by 24%; however, the additional gain achieved in final cumulative CO_2 storage is only17%..

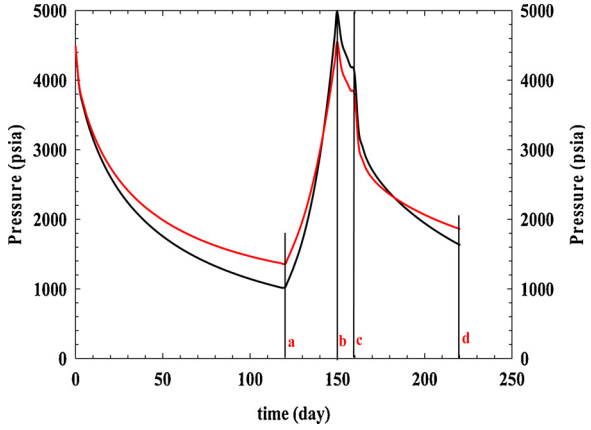

Fig. 8. Temporal variation of average reservoir pressure for a complete scenario consisting of primary depletion, CO_2 injection, soaking and secondary recovery with and without including the effect of sorption. Red curve shows a scenario with sorption and the black curve shows a scenario in the absence of sorption. Section (0-a) is primary production interval, (a–b) shows the injection period, (b–c) is the soaking time and (c–d) presents the secondary production period. Sorption causes the reservoir to deplete over longer time and slows down overpressurization of reservoir during the injection period.

drop as temperature increases. As can be viewed in Fig. 4, by increasing temperature from 35°*C* to 100°*C*,the initial CO_2 storage and CH_4 production rates reduce by almost 30%.The final CO_2 cumulative storage at the end of secondary production period enhances from 60% to 84% as shown in Fig. 5. It is quite obvious that lower-temperature shale gas reservoirs are better candidates for CO_2 storage, especially when the significant effect of adsorption is included, and the presented results herein match with the normal expectations.

4.3. Effect of Darcy (intrinsic) permeability on CO_2 sequestration and CH_4 recovery

The intrinsic permeabilities of 50, 100 and 200*nD* are selected to measure the sensitivity of CO_2-EGR to the variation of permeability at an initial reservoir pressure of 4500*psia*and reservoir temperature of 75°*C*. Fig. 6 shows the variation of CO_2 storage and CH_4 production rate with time at the above three fixed permeability values. It is worth noting that in the formulation of the governing equations presented in this paper, permeability has no direct effect on adsorption; however, it impacts the pore size in general and might actually affect adsorption indirectly. As observed in Fig. 6, lower intrinsic permeability results in higher CO_2 storage and methane production rates. To inject the same amount of CO_2 in the shale gas reservoir with a lower value of Darcy permeability, injection pressure must be higher and the increase in injection pressure causes the storage and production rates to grow.

Fig. 7 presents the normalized cumulative storage and production with time for the above set of scenarios. Reducing permeability by a factor of four, which is a quite high reduction, increases cumulative CO_2 storage from 66% to 83% in the shale gas reservoir at the temperature of 75°*C* and initial pressure of4500*psia*.

Among all the above scenarios, the maximum CO_2 cumulative storage at the end of secondary production period, which is 89.8% of the total injected CO_2, happens at the initial reservoir pressure of 5000*psia*,reservoir temperature of 75°*C*and Darcy permeability of 100*nD*. The maximum CH_4 cumulative production, which is 27.1% of the original methane in place, is observed at the initial reservoir pressure of 4500*psia*, reservoir temperature of 75°*C*and Darcy permeability of 50*nD*. It is worth noting that the recovery factor at the end of primary production for the above case is only 26%,compared to 65% of the base case, and the requirement to increase the injection pressure to a high degree is the cause of such a high additional methane recovery. The most

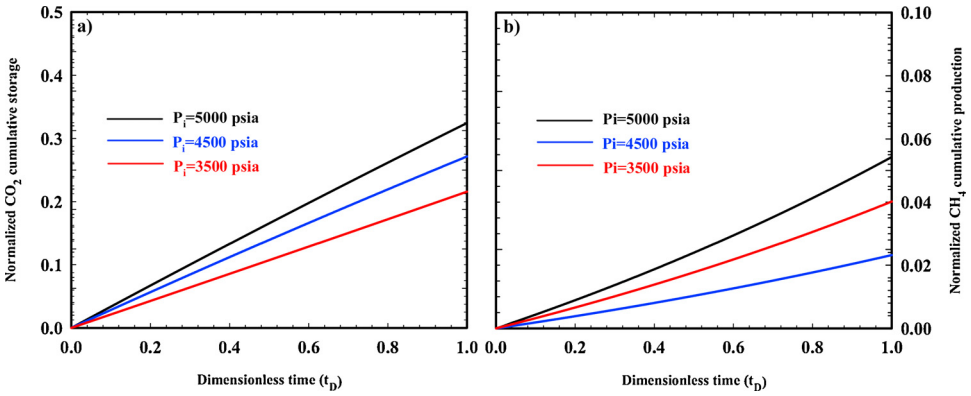

Fig. 9. Normalized cumulative CO_2 storage and CH_4 production versus time for three different reservoir initial pressures ignoring the effect of sorption; the maximum storage and recovery belong to the case with the highest initial pressure or equivalently highest injection pressure. The portion of adsorbed gas for the initial pressure of 5000*psia*is 55% in CO_2 storage and 7.8% in CH_4 additional recovery.

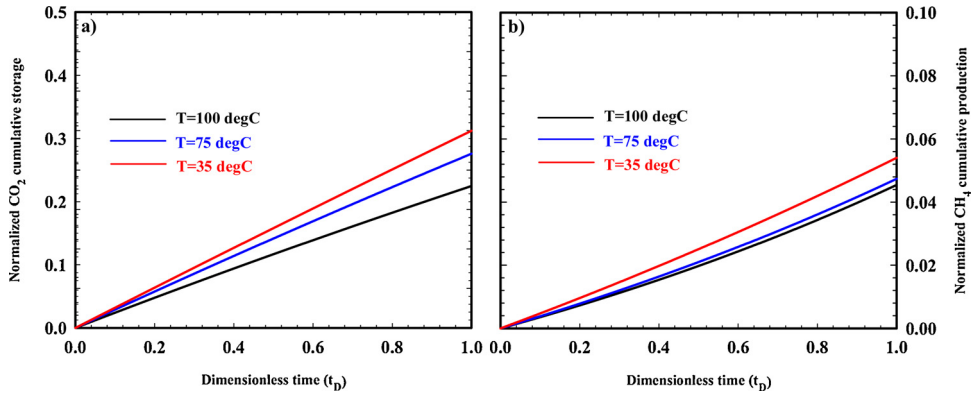

Fig. 10. Normalized cumulative CO_2 storage and CH_4 production versus time for three different reservoir temperatures ignoring the effect of sorption; the maximum storage and recovery belong to the case with the lowest temperature. The portion of adsorbed gas for the temperature of 35°*C*is 50.8% in CO_2 storage and 8.8% in CH_4 additional recovery.

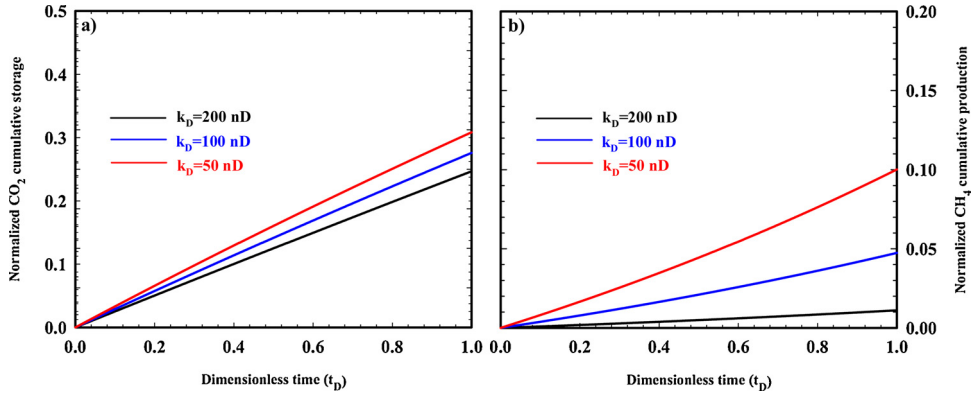

Fig. 11. Normalized cumulative CO_2 storage and CH_4 production versus time for three different reservoir intrinsic permeabilities ignoring the effect of sorption; the maximum storage and recovery belong to the case with the lowest permeability. The portion of adsorbed gas for the permeability of 50*nD*is 50.1% in CO_2 storage and 16.3% in CH_4 additional recovery.

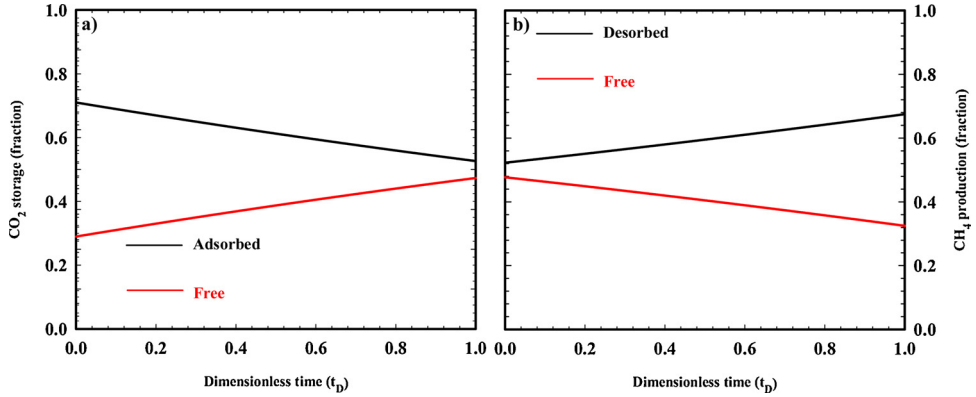

Fig. 12. The fraction of sorption and free gas in CO_2 storage and CH_4 recovery for the base case with an initial pressure of 4500*psia*,temperature of 75°*C* and Darcy permeability of 100*nD*. The fraction of sorption is in general more significant than that of free gas with a minimum ratio of 52: 48 and maximum ratio of.

influential parameter on CO_2 storage is the initial (injection) pressure.

4.4. Effect of sorption on CO_2 sequestration and CH_4 recovery

It is of high importance to investigate the sole effect of adsorption/desorption on CO_2 sequestration and enhanced methane recovery in partially depleted shale gas reservoirs. A large portion of injected CO_2 is stored in shale gas reservoirs due to the competitive adsorption of CO_2 over CH_4 and replacement of the latter by the former on shale surface. Shale gas reservoirs even if the adsorption effect were ignored would be categorized as unconventional reservoirs in which several mechanisms other than Darcy flow play role in fluid dynamics. The variation in average reservoir pressure over the whole simulation time is illustrated in Fig. 8. Including the effect of sorption in the simulations causes the pressure drop to happen more slowly during primary depletion; in other words sorption acts as a pressure support in the reservoir. The final pressure at the end of injection and also the soaking period is lower when sorption is involved while same amount of CO_2 is added to the reservoir in both scenarios. The average reservoir pressure is also in general higher over the secondary production period when sorption is activated.

To quantify the fraction of CO_2 trapped by sorption compared to

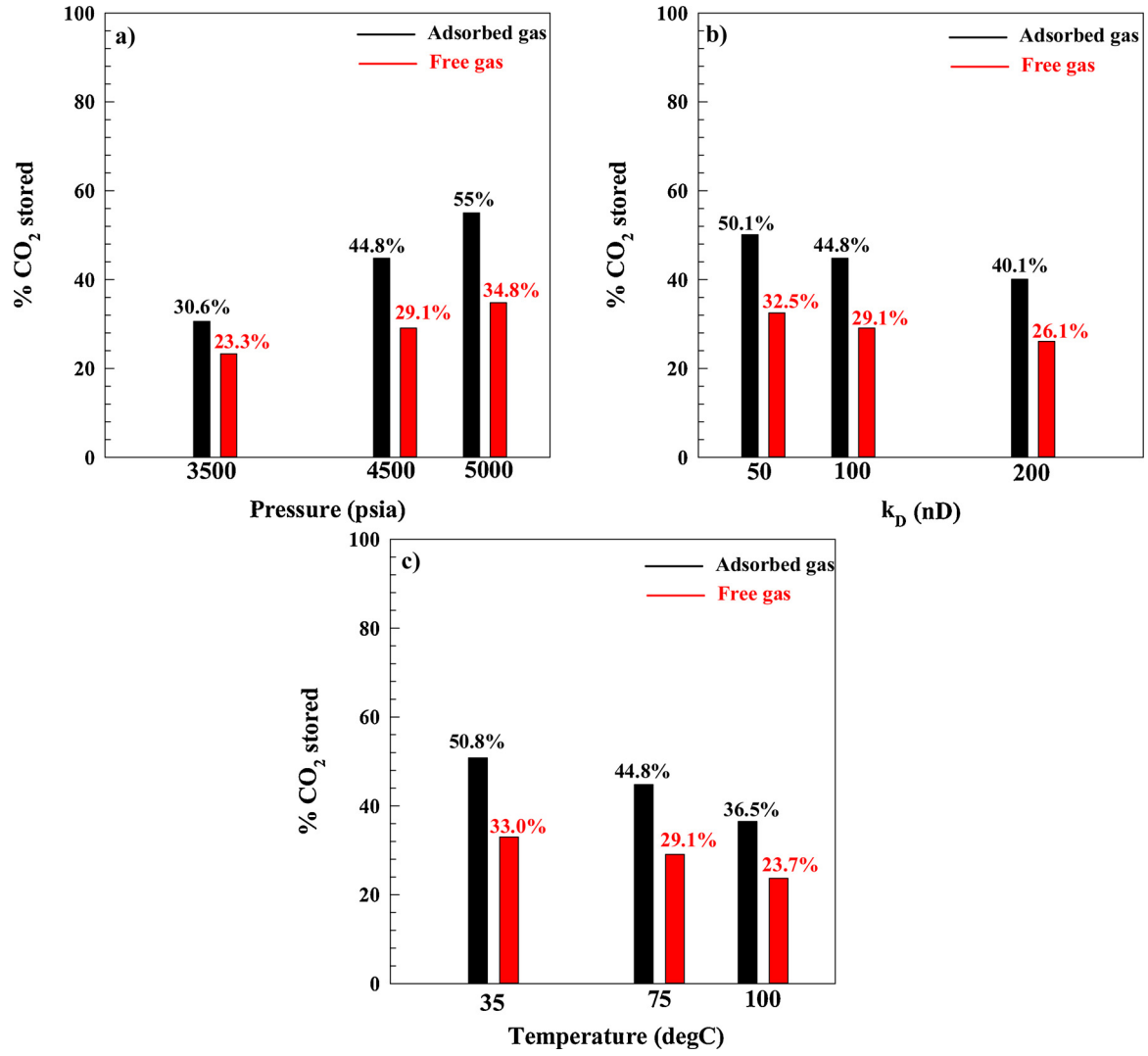

Fig. 13. The percentage of the total injected CO_2 which is stored and remained in the reservoir at the end of secondary production period showing the individual portions of adsorbed and free gas in **(a)** for different initial pressures at the temperature of $75°C$and permeability of $100nD$,in **(b)** for different Darcy permeabilities at the initial pressure of $4500psia$and temperature of $75°C$,and in **(c)** for different reservoir temperatures at the initial pressure of $4500psia$and permeability of.

that of free gas, the above set of experiments in the absence of sorption are simulated. For the sake of brevity, only the results of cumulative storage and production are presented here. The interesting point to consider is that although the nature of free and adsorbed gas are different, the trends are preserved, in the sense that the maximum CO_2 storage and maximum CH_4 production happen at the maximum initial reservoir pressure, minimum reservoir temperature and minimum intrinsic permeability when each of the above is taken as the sensitivity measure. In addition, the slope of the curves is greater when CO_2 storage or CH_4 production rate is higher. Figs. 9, 10 and 11 display the normalized cumulative storage and production for three different initial pressures, temperatures and Darcy permeabilities. The preservation of the trends can be attributed to the mechanisms other than adsorption involved in shale gas flow dynamics. Fig. 9 shows the normalized cumulative CO_2 storage and CH_4 production versus time for three different reservoir initial pressures in the absence of sorption. By Comparison to the scenario where sorption is included, the results of which are shown in Fig. 2, it is realized that sorption contributes to 55% additional storage and about 8% additional methane recovery. Fig. 10 shows the normalized cumulative CO_2 storage and CH_4 production versus time for three different reservoir temperatures in the absence of sorption. The results demonstrate that at a reservoir temperature of $35°C$sorption contributes to 50.8% additional CO_2 storage and 8.8% to CH_4 additional recovery. Fig. 11 shows the normalized cumulative CO_2 storage and CH_4 production versus time for three different reservoir intrinsic permeabilities ignoring the effect of sorption. For a permeability of $50nD$the adsorbed gas contributes to 50.1% in CO_2 storage and 16.3% in CH_4 additional recovery. For example, an influencing phenomenon is gas slippage. The value of slip coefficient is higher for CH_4 than that of CO_2, and as the pressure increases or permeability/temperature decreases, the difference between the two values becomes more noticeable. Slip coefficient is one of the important parameters which causes methane to be produced at a faster rate compared to other components and results in chromatographic separation in the shale medium.

In Fig. 12 the fractional rate of adsorbed and free CO_2 as well as the fractional rate of desorbed and free CH_4 for the base case are illustrated. The fractional rate of CO_2 is defined as the rate of adsorbed or free CO_2 divided by the average rate of CO_2 storage during secondary recovery. Also, the fractional rate of methane production is defined as the rate of desorbed or free methane divided by the average rate of methane production during secondary recovery. As can be viewed, with time or as the medium pressure decreases, the portion of adsorption in CO_2 storage drops (the fraction of free gas signifies) and the portion of desorption in CH_4 production increases (the fraction of free gas declines), however the role of sorption is more highlighted throughout the

whole simulation time.

The above results confirm and emphasize the necessity of including sorption mechanism in the simulations of shale gas flow, obtaining experimental sorption data for each specific shale sample and adding the proper modules to the existing reservoir simulators to prevent large errors in shale gas reservoirs production/storage forecast.

Last but not least, the contribution of adsorbed and free gas to the total stored CO_2 is presented in Fig. 13 versus initial pressure, Darcy permeability and reservoir temperature separately. As viewed and already mentioned, the portion of adsorbed gas is always higher than that of free gas. Adsorption is more noticeable at higher initial pressure, lower temperature and lower Darcy permeability. The trend (ascending/descending) of contribution to the storage is the same for adsorbed and free phase. The most changes occur over the pressure interval considered in this study, as the maximum and minimum storage among all the scenarios belong to the one with the maximum and minimum initial pressure, respectively. The tighter shale gas reservoirs with higher pressures and lower temperatures are better candidates from the viewpoint of CO_2 storage. The results reveal that depending on the pressure, temperature and reservoir permeability between $30 - 55\%$ of the injected CO_2 can be stored in shale gas reservoir in adsorbed form while the fraction of free gas is between $20 - 33\%$. Comparing trapping efficiency of CO_2-EGR with other methods of accelerating CO_2 dissolution in deep saline aquifers [46–52], adsorbed phase trapping is promising.

5. Summary and conclusions

A numerical model was developed to simulate multi-component gas flow in shale matrix blocks taking into account the simultaneous effects of all the major contributing mechanisms, namely viscous and slip flow, Knudsen diffusion, gas adsorption/desorption, pore enlargement, and real gas dynamics. The developed model was then utilized to simulate the process of carbon dioxide sequestration coupled with enhanced methane recovery and investigate the response of shale gas reservoirs to the variation of in-situ parameters such as pressure, temperature and reservoir permeability. Each scenario includes the periods of primary production, CO_2 injection, soaking and secondary production.

The results of CO_2 sequestration and CH_4 recovery are promising, especially from the viewpoint of storage which is shown to be far greater than additional methane recovery. A maximum storage of $\sim 90\%$ of the total injected CO_2 was observed in the shale reservoir with the initial pressure of $5000psia$, temperature of $75°C$ and permeability of $100nD$ where 55% of CO_2 was trapped as adsorbed phase. It was shown that CO_2 storage and CH_4 recovery are higher and change more rapidly at higher initial pressures, lower temperatures and lower permeabilities, which are the characteristics of a suitable shale gas reservoir candidate for CO_2-EGR. Pressure was found to be the most influential factor on storage and recovery. The contribution of adsorption to CO_2 storage and desorption to CH_4 production are significant and greater than that of the free phase; as the reservoir pressure declines the portion of the free and sorbed phase approach an equilibrium. It was shown that significant portion of the injected CO_2 (˜30 to 55%) can be stored in adsorbed form in shale gas reservoirs while improving methane recovery (8–16%) from shale gas reservoirs. This study forms a basis and guide to include the effects of all the above mechanisms, especially the sorption effect, in numerical reservoir simulators modelling gas production and CO_2 storage in shale gas reservoirs to estimate the potential of the reservoir from viewpoints of carbon storage and additional natural gas recovery.

Declaration of Competing Interest

The authors declare that they have no known competing financial interests or personal relationships that could have appeared to influence the work reported in this paper.

Acknowledgments

The authors would like to thank two referees for their constructive comments. The support of the Natural Sciences and Engineering Research Council of Canada (NSERC) and NSERC/Energi Simulation Industrial Research Chair in the Department of Chemical and Petroleum Engineering at the University of Calgary is acknowledged.

References

[1] R. Pachauri, A. Reisinger, Climate change 2007. Synthesis report, Contribution of Working Groups I, II and III to the Fourth Assessment Report, Cambridge University Press, Cambridge, 2008.
[2] W. Gunter, S. Wong, D. Cheel, G. Sjostrom, Large CO_2 sinks: their role in the mitigation of greenhouse gases from an international, national (Canadian) and provincial (Alberta) perspective, Appl. Energy 61 (4) (1998) 209–227.
[3] F. Luo, R.-N. Xu, P.-X. Jiang, Numerical investigation of the influence of vertical permeability heterogeneity in stratified formation and of injection/production well perforation placement on CO_2 geological storage with enhanced CH_4 recovery, Appl. Energy 102 (2013) 1314–1323.
[4] N. Mac Dowell, P.S. Fennell, N. Shah, G.C. Maitland, The role of CO_2 capture and utilization in mitigating climate change, Nat. Clim. Chang. 7 (4) (2017) 243.
[5] W. Ampomah, R. Balch, M. Cather, R. Will, D. Gunda, Z. Dai, M. Soltanian, Optimum design of CO_2 storage and oil recovery under geological uncertainty, Appl. Energy 195 (2017) 80–92.
[6] Z. Dai, H. Viswanathan, R. Middleton, F. Pan, W. Ampomah, C. Yang, W. Jia, T. Xiao, S.-Y. Lee, B. McPherson, CO_2 accounting and risk analysis for CO_2 sequestration at enhanced oil recovery sites, Environ. Sci. Technol. 50 (14) (2016) 7546–7554.
[7] Z. Dai, Y. Zhang, J. Bielicki, M.A. Amooie, M. Zhang, C. Yang, Y. Zou, W. Ampomah, T. Xiao, W. Jia, Heterogeneity-assisted carbon dioxide storage in marine sediments, Appl. Energy 225 (2018) 876–883.
[8] H. Emami-Meybodi, H. Hassanzadeh, C.P. Green, J. Ennis-King, Convective dissolution of CO_2 in saline aquifers: progress in modeling and experiments, Int. J. Greenh. Gas Control. 40 (2015) 238–266.
[9] I. Gray, Stress, gas, water and permeability-their interdependence and relation to outbursting, management and control of High gas emissions and outbursts in underground coal mines, International Symposium Cum Workshop (1995) 20–24.
[10] H. Dashti, L.Z. Yew, X. Lou, Recent advances in gas hydrate-based CO_2 capture, J. Nat. Gas Sci. Eng. 23 (2015) 195–207.
[11] Ş. Merey, Ç. Sınayuç, Experimental analysis of adsorption capacities and behaviors of shale samples, 19th International Petroleum and Natural Gas Congress and Exhibition of Turkey (2013).
[12] I. ETP, IEA Energy Technology Perspectives 2008–Scenarios and Strategies to 2050, International Energy Agency, IEA Publications, Paris, 2008.
[13] Technically Recoverable Shale Oil and Shale Gas Resources: an Assessment of 137 Shale Formations in 41 Countries Outsside the United States, Retrieved September, Energy Information Administration (EIA), 2013, p. 2013.
[14] J.F. Gale, J. Holder, Natural fractures in some US shales and their importance for gas production, Petroleum Geology Conference Series, Geological Society of London, Geological Society, London, 2010, pp. 1131–1140.
[15] M. Kok, S. Merey, Shale gas: current perspectives and future prospects in Turkey and the world, Energy Sources Part A Recovery Util. Environ. Eff. 36 (22) (2014) 2492–2501.
[16] J.B. Curtis, Fractured shale-gas systems, AAPG Bull. 86 (11) (2002) 1921–1938.
[17] S.B. Vellanki, Adsorption of Binary Gas Mixtures on Wet Fruitland Coal and Compressibility Factor Predictions, Oklahoma State University, 1995.
[18] D. Lancaster, D. Hill, A Multi-laboratory Comparison of Isotherm Measurements on Antrim Shale Samples, Otsego County, Michigan, SCA Paper (9303), (1993), p. 15.
[19] S. Rani, E. Padmanabhan, B.K. Prusty, Review of gas adsorption in shales for enhanced methane recovery and CO_2 storage, J. Pet. Sci. Eng. (2018).
[20] D. Liu, Y. Li, S. Yang, R.K. Agarwal, CO_2 sequestration with enhanced shale gas recovery, Energy Sources Part A Recovery Util. Environ. Eff. (2019) 1–11.
[21] M. Godec, G. Koperna, R. Petrusak, A. Oudinot, Enhanced gas recovery and CO_2 storage in gas shales: a summary review of its status and potential, Energy Procedia 63 (2014) 5849–5857.
[22] S.M. Kang, E. Fathi, R.J. Ambrose, I.Y. Akkutlu, R.F. Sigal, Carbon dioxide storage capacity of organic-rich shales, Spe J. 16 (04) (2011) 842–855.
[23] F. Tayari, S. Blumsack, R. Dilmore, S.D. Mohaghegh, Techno-economic assessment of industrial CO_2 storage in depleted shale gas reservoirs, J. Unconv. Oil Gas Resour. 11 (2015) 82–94.
[24] S.S.H. Boosari, U. Aybar, M.O. Eshkalak, Carbon dioxide storage and sequestration in unconventional shale reservoirs, J. Geosci. Environ. Prot. 3 (1) (2015) 7–15.
[25] P. Chareonsuppanimit, S.A. Mohammad, R.L. Robinson Jr., K.A. Gasem, High-pressure adsorption of gases on shales: Measurements and modeling, Int. J. Coal Geol. 95 (2012) 34–46.
[26] E. Fathi, I.Y. Akkutlu, Multi-component gas transport and adsorption effects during CO_2 injection and enhanced shale gas recovery, Int. J. Coal Geol. 123 (2014) 52–61.
[27] H. Sun, J. Yao, S.-h. Gao, D.-y. Fan, C.-c. Wang, Z.-x. Sun, Numerical study of CO_2 enhanced natural gas recovery and sequestration in shale gas reservoirs, Int. J. Greenh. Gas Control. 19 (2013) 406–419.
[28] Q. Zhang, Y. Su, W. Wang, M. Lu, G. Sheng, Gas transport behaviors in shale nanopores based on multiple mechanisms and macroscale modeling, Int. J. Heat Mass

Transf. 125 (2018) 845–857.
[29] F. Javadpour, Nanopores and apparent permeability of gas flow in mudrocks (shales and siltstone), J. Can. Pet. Technol. 48 (08) (2009) 16–21.
[30] R.G. Loucks, R.M. Reed, S.C. Ruppel, U. Hammes, Spectrum of pore types and networks in mudrocks and a descriptive classification for matrix-related mudrock pores, AAPG Bull. 96 (6) (2012) 1071–1098.
[31] C.-M. Ho, Y.-C. Tai, Micro-electro-mechanical-systems (MEMS) and fluid flows, Annu. Rev. Fluid Mech. 30 (1) (1998) 579–612.
[32] S. Roy, R. Raju, H.F. Chuang, B.A. Cruden, M. Meyyappan, Modeling gas flow through microchannels and nanopores, J. Appl. Phys. 93 (8) (2003) 4870–4879.
[33] F. Javadpour, D. Fisher, M. Unsworth, Nanoscale gas flow in shale gas sediments, J. Can. Pet. Technol. 46 (10) (2007).
[34] V. Swami, A.T. Settari, F. Javadpour, A numerical model for multi-mechanism flow in shale gas reservoirs with application to laboratory scale testing, EAGE Annual Conference & Exhibition Incorporating SPE Europec, Society of Petroleum Engineers (2013).
[35] H. Singh, F. Javadpour, Nonempirical apparent permeability of shale, Unconventional Resources Technology Conference (URTEC) (2013).
[36] V. Shabro, C. Torres-Verdin, F. Javadpour, Numerical simulation of shale-gas production: from pore-scale modeling of slip-flow, Knudsen diffusion, and langmuir desorption to reservoir modeling of compressible fluid, North American Unconventional Gas Conference and Exhibition, Society of Petroleum Engineers (2011) ss.
[37] C. Guo, M. Wei, H. Liu, Modeling of gas production from shale reservoirs considering multiple transport mechanisms, PLoS One 10 (12) (2015) e0143649.
[38] R. Evans III, G. Watson, E. Mason, Gaseous diffusion in porous media at uniform pressure, J. Chem. Phys. 35 (6) (1961) 2076–2083.
[39] E. Mohagheghian, H. Hassanzadeh, Z. Chen, Estimation of shale apparent permeability for multi-mechanistic multi-component gas production using rate transient analysis, Energy Fuels (2019).
[40] M. Rezaveisi, F. Javadpour, K. Sepehrnoori, Modeling chromatographic separation of produced gas in shale wells, Int. J. Coal Geol. 121 (2014) 110–122.
[41] A.L. Lee, M.H. Gonzalez, B.E. Eakin, The viscosity of natural gases, J. Pet. Technol. 18 (08) (1966) 997–1000.
[42] E.J. Peters, Advanced petrophysics, Geology, Porosity, Absolute Permeability, Heterogeneity and Geostatistics Volume 1 Live Oak Book Co, Austin, Texas, 2012.
[43] L. Shen, Z. Chen, Critical review of the impact of tortuosity on diffusion, Chem. Eng. Sci. 62 (14) (2007) 3748–3755.
[44] A. Agrawal, S. Prabhu, Survey on measurement of tangential momentum accommodation coefficient, J. Vac. Sci. Technol. A Vac. Surf. Films 26 (4) (2008) 634–645.
[45] S.W. Webb, K. Pruess, The use of Fick's law for modeling trace gas diffusion in porous media, Transp. Porous Media 51 (3) (2003) 327–341.
[46] Y. Leonenko, D.W. Keith, Reservoir engineering to accelerate the dissolution of CO_2 stored in aquifers, Environ. Sci. Technol. 42 (8) (2008) 2742–2747.
[47] H. Hassanzadeh, M. Pooladi-Darvish, D.W. Keith, Accelerating CO_2 dissolution in saline aquifers for geological storage-mechanistic and sensitivity studies, Energy Fuels 23 (6) (2009) 3328–3336.
[48] M. Zirrahi, H. Hassanzadeh, J. Abedi, The laboratory testing and scale-up of a downhole device for CO_2 dissolution acceleration, Int. J. Greenh. Gas Control. 16 (2013) 41–49.
[49] M. Zirrahi, H. Hassanzadeh, J. Abedi, Modeling of CO_2 dissolution by static mixers using back flow mixing approach with application to geological storage, Chem. Eng. Sci. 104 (2013) 10–16.
[50] M.J. Shafaei, J. Abedi, H. Hassanzadeh, Z. Chen, Reverse gas-lift technology for CO_2 storage into deep saline aquifers, Energy 45 (1) (2012) 840–849.
[51] S. Zendehboudi, A. Khan, S. Carlisle, Y. Leonenko, Ex situ dissolution of CO_2: a new engineering methodology based on mass-transfer perspective for enhancement of CO_2 sequestration, Energy Fuels 25 (7) (2011) 3323–3333.
[52] S. Zendehboudi, A. Shafiei, A. Bahadori, Y. Leonenko, I. Chatzis, Droplets evolution during ex situ dissolution technique for geological CO_2 sequestration: experimental and mathematical modelling, Int. J. Greenh. Gas Control. 13 (2013) 201–214.